*Briefings in Bioinformatics*, 2024, pp. 1–13

doi: DOI HERE
Advance Access Publication Date: Day Month Year
Problem Solving Protocol

PROBLEM SOLVING PROTOCOL

# Graph Contrastive Learning as a Versatile Foundation for Advanced scRNA-seq Data Analysis

Zhenhao Zhang,[1,2] Yuxi Liu,[3] Meichen Xiao,[1] Kun Wang,[1] Yu Huang,[3] Jiang Bian,[3] Ruolin Yang[1,*] and Fuyi Li[1,2,*]

[1]College of Life Sciences, Northwest A&F University, Yangling, 712100, Shaanxi, China, [2]College of Information Engineering, Northwest A&F University, Yangling, 712100, Shaanxi, China and [3]College of Medicine, University of Florida, Gainesville, 32610, FL, USA
[*]Corresponding author. desert.ruolin@gmail.com and fuyi.li@nwafu.edu.cn
FOR PUBLISHER ONLY Received on Date Month Year; revised on Date Month Year; accepted on Date Month Year

## Abstract

Single-cell RNA sequencing (scRNA-seq) offers unprecedented insights into transcriptome-wide gene expression at the single-cell level. Cell clustering has been long established in the analysis of scRNA-seq data to identify the groups of cells with similar expression profiles. However, cell clustering is technically challenging, as raw scRNA-seq data have various analytical issues, including high dimensionality and dropout values. Existing research has developed deep learning models, such as graph machine learning models and contrastive learning-based models, for cell clustering using scRNA-seq data and has summarized the unsupervised learning of cell clustering into a human-interpretable format. While advances in cell clustering have been profound, we are no closer to finding a simple yet effective framework for learning high-quality representations necessary for robust clustering. In this study, we propose scSimGCL, a novel framework based on the graph contrastive learning paradigm for self-supervised pretraining of graph neural networks. This framework facilitates the generation of high-quality representations crucial for cell clustering. Our scSimGCL incorporates cell-cell graph structure and contrastive learning to enhance the performance of cell clustering. Extensive experimental results on simulated and real scRNA-seq datasets suggest the superiority of the proposed scSimGCL. Moreover, clustering assignment analysis confirms the general applicability of scSimGCL, including state-of-the-art clustering algorithms. Further, ablation study and hyperparameter analysis suggest the efficacy of our network architecture with the robustness of decisions in the self-supervised learning setting. The proposed scSimGCL can serve as a foundation model for practitioners developing tools for cell clustering. The source code of scSimGCL is publicly available at `https://github.com/zhangzh1328/scSimGCL`.

**Key words:** scRNA-seq data, graph contrastive learning, self-supervised learning, cell-cell graph, cell clustering

## Introduction

Cells are essential building blocks of all living organisms and play a pivotal role in a myriad of biological functions. The heterogeneity in gene expression across individual cells has emerged as a significant field of study, especially with the development of single-cell RNA sequencing (scRNA-seq). The scRNA-seq, perhaps the most widely used method for transcriptome-wide analysis at the single-cell level [1], allows a deeper insight into cell classification, characterization, and differentiation. Such analysis have successfully uncovered the complex association between cellular functions and improved the performance of various downstream applications. These applications include profiling genetic diversity within populations [46], identifying and annotating cell subtypes [40], and facilitating advances in drug discovery and development [28].

However, raw scRNA-seq data present their own set of challenges, such as high dimensionality and measurement noise [21]. Notably, measurement noise often causes dropout events, where genes appear to be unexpressed due to technical artifacts rather than biological reality. Recent advancements in deep learning techniques have shown promise in addressing these challenges by reducing the dimensionality of data and filtering out the noise to uncover biological signals. Deep learning techniques have been widely used in bioinformatics, including scRNA-seq data analysis, to provide new insights into cellular functions.

In the realm of scRNA-seq data analysis, deep neural networks have been usefully explored. Prior studies by [25, 16, 7, 41, 26] have employed autoencoders – a type of neural network to effectively learn condensed representations of scRNA-seq data in a lower-dimensional space. Representative examples of scDeepCluster, DESC, and scDCC [25, 16,

Zhenhao and Yuxi are equal contributors to this work.

© The Author 2024. Published by Oxford University Press. All rights reserved. For permissions, please e-mail: journals.permissions@oup.com

26], which are specifically designed to provide clustering assignments with scRNA-seq data. Such approaches, DCA and scGMAI [7, 41], integrate data imputation into their clustering assignments to mitigate the impact of dropout events, thereby facilitating the formation of informative gene expression matrices, which is essential for improving cell clustering.

More recent studies have seen increasingly rapid advances in the field of scRNA-seq data analysis [6, 34, 4, 5, 32, 8]. On the one hand, graph-sc, scASGC, and scGAC [6, 34, 4] employ graph autoencoders to encode scRNA-seq data as cell graphs and capture the between-cell association. On the other hand, contrastive-sc, scDCCA, and scDECL [5, 32, 8] focus on the provision of autoencoder with contrastive learning. The intuition behind contrastive learning is to compare input samples in order to learn desirable representations using the similarity between positive pairs or the dissimilarity between negative pairs. Accordingly, contrastive learning is recognized as an alternative approach to reconstruction-based with a focus on learning an embedding space where similar ones are pushed closer to each other while dissimilar ones are pushed farther apart [27].

Despite these promising advances, research has yet to systematically develop a simple yet effective framework for learning high-quality representations crucial for robust cell clustering. The learning of high-quality representations is built upon the success of pretraining generalizable models, which aligns with the promise of the current foundation models (i.e., a series of large-scale pretrained models that can be applied on various downstream use cases and tasks) [19, 36, 20]. The foundation model has been instrumental in our understanding of the role of deep learning in the biological context. However, the transition to practical, actionable insights in scRNA-seq remains challenging, especially in analyzing and interpreting complex biological data.

To bridge this gap, we incorporate the graph contrastive learning (GCL) paradigm into scRNA-seq data analysis. Several key aspects of modeling need to be carefully considered. First, the construction of cell-cell graphs from scRNA-seq data presents a fundamental challenge. Second, there is an urgent need to design a neural network architecture that leverages the GCL paradigm to learn representations desirable for cell-cell graphs. Third, the development of pretraining strategies as a pretext task in the self-supervised learning setting is critical for improving the effectiveness and robustness of the model decisions.

In this study, we propose scSimGCL, a simple and effective framework that combines graph neural networks with contrastive learning, aligning with the GCL paradigm, specifically tailored for scRNA-seq data analysis. The GCL paradigm facilitates self-supervised pretraining of graph neural networks, which enables the generation of high-quality representations crucial for robust cell clustering. A critical component of our scSimGCL is the innovative construction of cell-cell graphs using scRNA-seq data. We develop a cell-cell graph structure learning mechanism that pays attention to the critical parts of the input data using a multi-head attention module [30] for improving the accuracy and relevance of graphs. This module is used for the purpose of deriving a nuanced cell-cell graph, where individual cells form nodes and their biological associations are represented as edges.

Moreover, our study addresses a major issue in existing methods that combine graph machine learning with contrastive learning for scRNA-seq data. Prior studies [13, 24, 39] often directly integrate preprocessed cell graphs (e.g., via K-Means) into the contrastive learning scheme. However, this method is likely to disrupt the intrinsic homophily of the graph, where connected nodes are expected to share similar properties, thus resulting in inferior quality of representation. In response to this issue, our approach adopts an effective strategy for constructing the pairs of contrastive learning using the homophily of original and augmented cell-cell graphs (generated by gene masking and edge dropping [18]). This strategy preserves the internal structure of graphs, facilitating the generation of informative contrastive pairs. Further, our approach introduces a well-designed pretraining mechanism to explore the topological nuances of cell-cell graphs. This mechanism implements contrastive learning with data imputation in a joint learning strategy, enhancing the model performance across various evaluation metrics.

We conduct rigorous evaluations of scSimGCL against deep learning approaches on both simulated and real scRNA-seq datasets. Our framework outperforms competing state-of-the-art models in scRNA-seq data imputation and cell clustering by a considerable margin. Further experimental investigations into the clustering assignments reveal that scSimGCL can seamlessly integrate state-of-the-art clustering algorithms into its architecture. Notably, the model is capable of making informed decisions by indicating "I know" and "I do not know" the number of clusters (i.e., K-Means and Affinity Propagation), which is a key aspect in unsupervised learning scenarios such as scRNA-seq data analysis. Ablation study and hyperparameter analysis further confirm the efficacy and robustness of scSimGCL in the self-supervised learning setting.

## Materials and methods

### The framework of scSimGCL

The overall structure of the proposed scSimGCL is illustrated in Figure 1. First, we incorporate a multi-head attention module [30] to learn a cell-cell graph from scRNA-seq data. Second, we adopt feature/gene masking and edge dropping in the learned cell-cell graph to generate its counterpart. Subsequently, the learned cell-cell graph and its counterpart are used to create contrastive pairs. Last, we design a pretraining mechanism to generate high-quality representations for cell clustering, where contrastive learning and data imputation are implemented with a joint learning strategy.

### Cell-cell graph structure learning

Let $\mathcal{G} = (\mathcal{V}, \mathcal{E}, \mathrm{X}) = (\mathrm{A}, \mathrm{X})$ be a cell-cell graph. $\mathcal{V} = \{v_1, v_2, \cdots, v_N\}$ is a collection of nodes, where each is a cell and $N$ is the number of cells. $\mathcal{E}$ is a collection of edges between nodes. $\mathrm{X} \in \mathbb{R}^{N \times g}$ is the gene expression matrix obtained after preprocessing, where $g$ is the number of genes. The genes with zero values in $X$ are denoted by using a mask matrix $\mathrm{M} \in \mathbb{R}^{N \times g}$. The aim of cell-cell graph structure learning is to obtain an adjacency matrix $A \in [0, 1]^{N \times N}$ using scRNA-seq data, where $A_{ij} \in [0, 1]$ denotes the edge between cells $i$ and $j$. In order to obtain the adjacency matrix $A$, we incorporate a multi-head attention module [30] into the network architecture. Specifically, query $Q$ and key $K$ vectors are generated using a linear transformation on $X$. The dot product is carried out between $Q$ and $K$, using the Softmax function to obtain up to $m$ attention heads. All heads are concatenated and then projected using a linear transformation to the original space. The mathematical formulation of the above process is

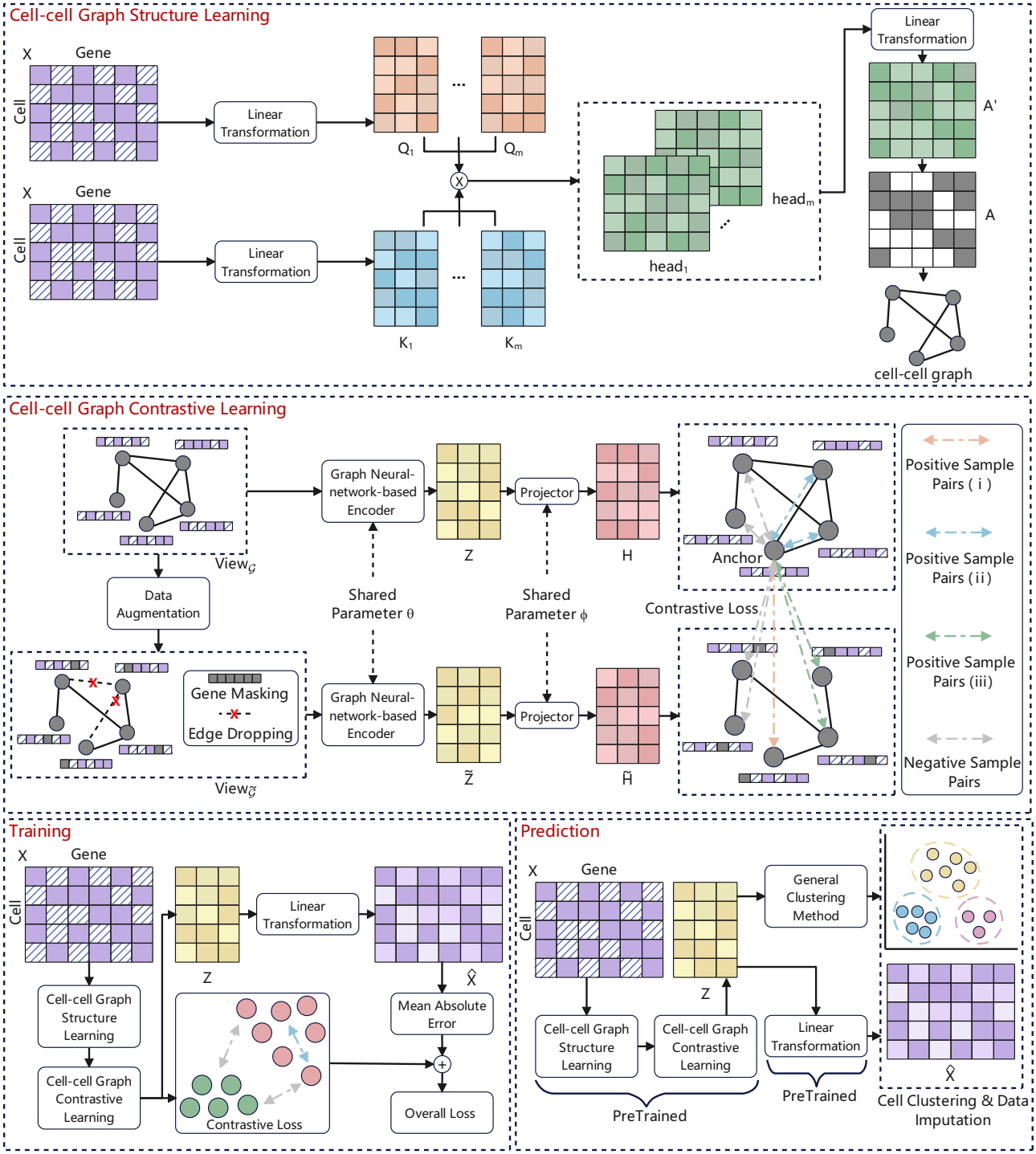


**Fig. 1. The overall framework of scSimGCL, which includes cell-cell graph structure and contrastive learning that take into account the contributions of cell-cell graph representations for cell clustering.**

as follows:

$$
\begin{aligned}
&\mathrm{Q_i} = \mathrm{W_i^Q} \cdot \mathrm{X}, \mathrm{K_i} = \mathrm{W_i^K} \cdot \mathrm{X}, \\
&\mathrm{head}_i(\mathrm{X}) = \mathrm{softmax}\left(\frac{\mathrm{Q}_i \cdot \mathrm{K}_i^\top}{\sqrt{d_K}}\right), \\
&\mathrm{A}' = \mathrm{MultiHeadAtt}(\mathrm{X}), \\
&= [\mathrm{head}_1(\mathrm{X}) \oplus \cdots \oplus \mathrm{head}_i(\mathrm{X}) \oplus \cdots \oplus \mathrm{head}_m(\mathrm{X})]\, \mathrm{W}_O,
\end{aligned}
\tag{1}
$$

where $head_i$ is the i-th attention head. $\oplus$ is the concatenation. $d_K$ is the dimension of $K$. Accordingly, a sparse and non-negative adjacency matrix $A$ can be obtained using the intermediate matrix $\mathrm{A}'$ with numerical constraints as:

$$
\mathrm{A} = \begin{cases} 1, & \mathrm{A}' \geqslant \eta \\ 0, & \mathrm{A}' < \eta \end{cases},
\tag{2}
$$

where $\eta$ is a learnable threshold that excludes the values lower than that.

## Cell-cell graph contrastive learning

Data augmentation techniques allow the construction of counterparts from data samples. A data augmentation module is an important component in the GCL paradigm and plays a vital role in increasing the diversity of input graph samples [44]. We adopt attribute/gene masking and edge dropping [18] in the learned cell-cell graph to generate its counterpart. Specifically, we implement edge dropping by randomly dropping a collection of edges from the cell-cell graph. Given the adjacency matrix $A$, a masking matrix $\mathrm{M}^{(a)} \in [0,1]^{N\times N}$ is used here, where each $M_{ij}^{(a)}$ is derived from a Bernoulli distribution with probability $p^{(a)}$ independently. Accordingly, a new $\tilde{\mathrm{A}}$ can be derived from using $A$ with $M$ as:

$$\begin{aligned} \mathrm{M}_{ij}^{(a)} &\sim \text{Bernoulli}\left(p^{(a)}\right) \\ \tilde{\mathrm{A}} &= \mathrm{M}^{(a)} \odot \mathrm{A} \end{aligned}. \tag{3}$$

We implement gene masking by randomly masking a collection of genes with zero values from the cell-cell graph. In the same vein, a random vector $\mathrm{M}^{(x)} \in [0,1]^{g}$ is used here, where each is derived from a Bernoulli distribution with probability $p^{(x)}$ independently. Subsequently, the gene vector of each cell is masked with $\mathrm{M}^{(x)}$ and the gene matrix $\tilde{\mathrm{X}}$ is generated as:

$$\tilde{\mathrm{X}} = \left[\mathrm{X}_1 \odot \mathrm{M}^{(x)}, \mathrm{X}_2 \odot \mathrm{M}^{(x)}, \cdots, \mathrm{X}_N \odot \mathrm{M}^{(x)}\right]^{\top}. \tag{4}$$

The outputs of the above process are $\tilde{\mathrm{A}}$ and $\tilde{\mathrm{X}}$. The two cell-cell graphs $\mathcal{G} = (\mathcal{A}, \mathrm{X})$ and $\tilde{\mathcal{G}} = (\tilde{\mathcal{A}}, \tilde{\mathrm{X}})$ can be regarded as two graph views $View_{\mathcal{G}}$ and $View_{\tilde{\mathcal{G}}}$ for contrastive learning. Before implementing contrastive learning, we employ a graph neural network-based encoder $f_\theta(\cdot)$ to generate node/cell representations as:

$$\begin{aligned} \mathrm{Z} &= f_\theta(\mathcal{G}) = \mathrm{ReLU}\left(\mathrm{A}\,\mathrm{ReLU}\left(\mathrm{AXW}_1^{\mathrm{Z}}\right)\mathrm{W}_2^{\mathrm{Z}}\right) \\ \tilde{\mathrm{Z}} &= f_\theta(\tilde{\mathcal{G}}) = \mathrm{ReLU}\left(\tilde{\mathrm{A}}\,\mathrm{ReLU}\left(\tilde{\mathrm{A}}\tilde{\mathrm{X}}\mathrm{W}_1^{\mathrm{Z}}\right)\mathrm{W}_2^{\mathrm{Z}}\right) \end{aligned}, \tag{5}$$

where $\theta$ is the parameter of $f_\theta(\cdot)$. $Z$ and $\tilde{Z}$ are cell representations for both $View_{\mathcal{G}}$ and $View_{\tilde{\mathcal{G}}}$. The graph neural network-based encoder employed here is graph convolutional networks [12]. Subsequently, a projector $f_\phi(\cdot)$ is used to map the generated cell representations Z and $\tilde{\mathrm{Z}}$ into a lower-dimensional latent space as:

$$\begin{aligned} \mathrm{H} &= f_\phi(\mathrm{Z}) = \mathrm{W}^{\mathrm{H}} \cdot \mathrm{Z} + \mathrm{b}^{\mathrm{H}}, \\ \tilde{\mathrm{H}} &= f_\phi(\tilde{\mathrm{Z}}) = \mathrm{W}^{\mathrm{H}} \cdot \tilde{\mathrm{Z}} + \mathrm{b}^{\mathrm{H}}, \end{aligned} \tag{6}$$

where $\phi$ is the parameter of $f_\phi(\cdot)$. $H$ and $\tilde{H}$ are cell representations obtained after projection. The projector used here is built upon a natural Multi-Layer Perceptrons. Through the aforementioned steps, cell representations $H$ and $\tilde{H}$ are required to the implementation of contrastive learning are done.

Contrastive learning aims to maximize $H$ and $\tilde{H}$ mutual information. A node/cell is arbitrarily chosen from the learned cell-cell graph view as an anchor. The positive sample pairs for contrastive learning are as follows: (i) the nodes connected to the anchor, (ii) the anchor counterpart in its counterpart view, and (iii) the nodes connected to the anchor from its counterpart view, while negative samples are the remaining samples. The i-th cell in $View_{\mathcal{G}}$ is taken as the anchor and thus the contrastive loss $\mathcal{L}_i^{(\mathrm{gcl})}(\mathrm{H}, \mathrm{View}_{\mathcal{G}})$ as:

$$\begin{aligned} &\mathcal{L}_i^{(\mathrm{gcl})}(\mathrm{H}, \mathrm{View}_{\mathcal{G}}) = \\ &-\frac{1}{2|\mathcal{N}(i)|+1}\log\frac{\exp\left(f_\varphi\left(\mathrm{H}_i, \tilde{\mathrm{H}}_i\right)/\tau\right)+}{\exp\left(f_\varphi\left(\mathrm{H}_i, \tilde{\mathrm{H}}_i\right)/\tau\right)+} \\ &\frac{\sum_{v_j\in\mathcal{N}(i)}\left(\exp\left(f_\varphi\left(\mathrm{H}_i, \mathrm{H}_j\right)/\tau\right)+\exp\left(f_\varphi\left(\mathrm{H}_i, \tilde{\mathrm{H}}_j\right)/\tau\right)\right)}{\sum_{j\neq i}\left(\exp\left(f_\varphi\left(\mathrm{H}_i, \mathrm{H}_j\right)/\tau\right)+\exp\left(f_\varphi\left(\mathrm{H}_i, \tilde{\mathrm{H}}_j\right)/\tau\right)\right)} \end{aligned}, \tag{7}$$

where $\mathcal{N}(i)$ is a collection of neighbors for the i-th cell in $\mathcal{G}$. $f_\varphi(\cdot)$ is the measurement of similarity, and the dot product is carried out here $f_\varphi(a,b) = a \cdot b$. $\tau$ is a temperature parameter that provides the penalty for negative pairs.

Since we have two graph views $View_{\mathcal{G}}$ and $View_{\tilde{\mathcal{G}}}$ used for contrastive learning, the i-th cell in $View_{\tilde{\mathcal{G}}}$ is chosen as an anchor again. The contrastive loss $\mathcal{L}_i^{(\mathrm{gcl})}\left(\tilde{\mathrm{H}}, \mathrm{View}_{\tilde{\mathcal{G}}}\right)$ is computed by the way used in Eq. (7). Accordingly, the contrastive loss between $H$ and $\tilde{H}$ as:

$$\begin{aligned} \mathcal{L}^{(gcl)} = \alpha \cdot \frac{1}{N}\sum_{i=1}^{N}\mathcal{L}_i^{(gcl)}(\mathrm{H}, View_{\mathcal{G}}) + \\ \beta \cdot \frac{1}{N}\sum_{i=1}^{N}\mathcal{L}_i^{(gcl)}(\tilde{\mathrm{H}}, View_{\tilde{\mathcal{G}}}), \end{aligned} \tag{8}$$

where $\alpha$ and $\beta$ are two scaling parameters that take into account the contributions of the two losses.

## Training and Prediction

We design a pretraining mechanism to explore the topological nuances of cell-cell graphs. This mechanism implements contrastive learning with data imputation in a joint learning strategy. We have obtained contrastive learning loss $\mathcal{L}^{(gcl)}$ from the above section. Now, the imputation loss $\mathcal{L}^{(imp)}$ needs to be formulated. The cell representation $Z$ for $View_{\mathcal{G}}$ is used for scRNA-seq data imputation as:

$$\hat{\mathrm{X}} = \mathrm{W}^{\mathrm{x}} \cdot \mathrm{Z} + \mathrm{b}^{\mathrm{x}}, \tag{9}$$

where $\hat{X}$ is the obtained scRNA-seq data after predicting. The imputation of scRNA-seq data is a regression task, and thus the mean absolute error between $X$ and $\hat{X}$ of each cell as:

$$\mathcal{L}^{(imp)} = \frac{1}{N}\sum_{i=1}^{N}\left|\mathrm{X}_i \odot \mathrm{M}_\mathrm{i} - \hat{\mathrm{X}}_\mathrm{i} \odot \mathrm{M}_i\right|. \tag{10}$$

Next, we integrate both $\mathcal{L}^{(gcl)}$ and $\mathcal{L}^{(imp)}$ losses into an overall loss as:

$$\mathcal{L} = \mathcal{L}^{(imp)} + \lambda \cdot \mathcal{L}^{(gcl)}, \tag{11}$$

where $\lambda$ is a scaling parameter that takes into account the contributions of $\mathcal{L}^{(imp)}$ and $\mathcal{L}^{(gcl)}$.

In summary, through the obtained cell representation $Z$, a general clustering method can be employed to carry out clustering assignments. Accordingly, the two stages, cell representation learning and clustering assignment analysis, are decoupled in the proposed scSimGCL framework. By doing this, our scSimGCL framework provides more flexibility in implementing different clustering algorithms (K-Means and Affinity Propagation).

## Data

We evaluate the proposed scSimGCL against competing deep learning approaches on simulated and real scRNA-seq datasets. We compare scSimGCL with state-of-the-art models on both scRNA-seq data imputation and cell clustering tasks. The six scRNA-seq datasets used are Shekhar mouse retina cells [22], Baron [2], 10X PBMC [45], Camp [3], Mouse bladder cells [9], and Zeisel [43]. Each dataset is a form of two-dimensional matrix, where rows and columns are cells and genes, and each cell has its own available label. These datasets were processed using the Scanpy toolkit [35]. It includes excluding genes with expression values of zero from all cells first and then performing the normalization and logarithmically transformation on the gene expression matrix. The results obtained from the preliminary analysis of the six datasets are set out in Table 1.

**Table 1.** Results of the preliminary analysis on the six datasets.

| Dataset | No. of cells | No. of genes | No. of cell types |
|---|---|---|---|
| Shekhar mouse retina cells | 27499 | 13166 | 19 |
| Baron | 8569 | 20125 | 14 |
| 10X PBMC | 4340 | 33694 | 8 |
| Camp | 777 | 16270 | 7 |
| Mouse bladder cells | 2746 | 20670 | 16 |
| Zeisel | 3005 | 19972 | 9 |

The simulated scRNA-seq data is derived from the implementation of the Splatter [42] toolkit. There are up to twelve simulated datasets created for three case studies. This includes the simulation of (i) the drop events in the gene expression matrix, (ii) the strength of low signals for clustering assignments, and (iii) the high dimensionality of the gene expression matrix under extremely sparsity space. In order to implement the case study with varied dropout rates, we set the value of dropout.mid from 0 to 2, i.e., 0.0, 0.5, 1.0, 1.5, and 2.0. Meanwhile, the number of cells is set to 6000 with up to 4 clusters, the number of genes is set to 5000, and dropout.shape and de.fracScale are set to -1 and 0.3, respectively. In order to implement the case study with the different strengths of low signals (Sigma), we set the value of de.fracScale from 0.1 to 0.25, i.e., 0.1, 0.15, 0.2, and 0.25. Meanwhile, the number of cells is set to 6000 with up to 4 clusters, the number of genes is set to 5000, and dropout.shape and dropout.mid are set to -1 and 0, respectively. In order to implement the case study with varied dimension sizes under extremely sparsity space, we set the number of genes from 10000 to 20000, i.e., 10000, 15000, and 20000, and the value of dropout.mid to 2. Meanwhile, the number of cells is set to 6000 with up to 4 clusters, the number of genes is set to 5000, and dropout.shape and de.fracScale are set to -1 and 0.3, respectively.

## Evaluation

The clustering accuracy (CA) [38], normalized mutual information (NMI) [23], and adjusted rand index (ARI) [11] are utilized to assess the performance of clustering assignments. Accordingly, the CA between the predicted cell type $\hat{Y}$ with $N_{\hat{Y}}$ clusters and the ground truth $Y$ with $N_Y$ clusters as:

$$CA = \max_{\psi} \frac{\sum_{i=1}^{N} \mathbb{1}_{[Y_i=\psi(\hat{Y}_i)]}}{N}, \tag{12}$$

where $N$ is the number of cells. $\psi$ is a function that makes a transition between $\hat{Y}$ and $Y$. $\mathbb{1}_{[\cdot]}$ is an indicator function. The NMI between $\hat{Y}$ and $Y$ as:

$$NMI = \frac{\sum_{i=1}^{N_{\hat{Y}}} \sum_{j=1}^{N_Y} |\hat{Y}_i \bigcap Y_j| log \frac{N \times |\hat{Y}_i \bigcap Y_j|}{|\hat{Y}_i| \times |Y_j|}}{max(-\sum_{i=1}^{N_{\hat{Y}}} |\hat{Y}_i| log \frac{|\hat{Y}_i|}{N}, -\sum_{j=1}^{N_Y} |Y_j| log \frac{|Y_j|}{N})}. \tag{13}$$

The ARI between $\hat{Y}$ and $Y$ as:

$$ARI = \frac{\sum_{i=1}^{N_{\hat{Y}}} \sum_{j=1}^{N_Y} \begin{pmatrix} |\hat{Y}_i \cap Y_j| \\ 2 \end{pmatrix}}{\frac{1}{2}\left[\sum_{i=1}^{N_{\hat{Y}}} \begin{pmatrix} |\hat{Y}_i| \\ 2 \end{pmatrix} + \sum_{j=1}^{N_Y} \begin{pmatrix} |Y_j| \\ 2 \end{pmatrix}\right]} \frac{-\left[\sum_{i=1}^{N_{\hat{Y}}} \begin{pmatrix} |\hat{Y}_i| \\ 2 \end{pmatrix} \sum_{j=1}^{N_Y} \begin{pmatrix} |Y_j| \\ 2 \end{pmatrix}\right] / \begin{pmatrix} N \\ 2 \end{pmatrix}}{-\left[\sum_{i=1}^{N_{\hat{Y}}} \begin{pmatrix} |\hat{Y}_i| \\ 2 \end{pmatrix} \sum_{j=1}^{N_Y} \begin{pmatrix} |Y_j| \\ 2 \end{pmatrix}\right] / \begin{pmatrix} N \\ 2 \end{pmatrix}}. \tag{14}$$

The Pearson correlation coefficients (PCCs) is employed to assess the performance of scRNA-seq data imputation as:

$$PCCs = \frac{E(\hat{X}X) - E(\hat{X})E(X)}{\sqrt{E(\hat{X}^2) - E(\hat{X})^2} + \sqrt{E(X^2) - E(X)^2}}, \tag{15}$$

where $E(\cdot)$ is the expected value. $\hat{X}$ is the imputed value. $X$ is the ground truth.

# Results and discussion

## Performance comparison with baselines

We evaluate our scSimGCL against competing clustering approaches on six real scRNA-seq datasets. The clustering approaches employed in this study are scDCCA [32], scGNN [33], graph-sc [6], CIDR [17], SIMLR [31], and K-Means. The scDCCA is a combination of an autoencoder module and a contrastive learning module and focuses particularly on cell clustering. The scGNN comprises three stacked autoencoders and focuses on the provision of scRNA-seq data imputation and cell clustering. The graph-sc is built upon a graph autoencoder and focuses particularly on cell clustering. The CIDR is a statistical model that includes reducing the impact of the high dimensionality of scRNA-seq data using principal component analysis on cell clustering. The SIMLR is built upon multi-kernel learning that performs dimension reduction and cell clustering by measuring cell similarity in scRNA-seq data. We run all methods ten times and present the average CA, NMI, and ARI scores.

Figure 2 compares the CA, NMI, and ARI scores for each approach. We observed that the proposed scSimGCL consistently surpasses the baselines in terms of CA, NMI, and ARI scores. Significant improvement in our scSimGCL was found compared with K-Means. This result verifies the efficacy of our network architecture, which can generate high-quality representations and improve the performance of cell clustering. Looking at Figure 2, it is apparent that scDCCA is the best baseline that reported significantly more CA, NMI, and ARI scores than the other approaches (except for the Camp dataset). Interestingly, the K-Means was observed to achieve the best accuracy on the Camp dataset compared to other baselines. This result may partly be explained by the fact that the performance of deep learning-based models (i.e., scDCCA, scGNN, and graph-sc) is influenced by the input data size. As can be seen from the table (above), the Camp dataset contains

a small sample size among the six real scRNA-seq datasets. We run all methods ten times and present the average CA, NMI, and ARI scores.

Figure 3 compares the results obtained from the clustering assignment of all baselines and our scSimGCL on twelve simulated scRNA-seq datasets. These results are average values obtained by running all approaches ten times. Our scSimGCL consistently achieves the competing CA, NMI, and ARI scores compared with baselines. After zooming on the subgraphs with varied dropout rates, we observed that there is an overlap between graph-sc and our scSimGCL. Thus, graph-sc is the best baseline, and it reported significantly more CA, NMI, and ARI scores than the other approaches. Moreover, graph-sc was observed to achieve the best accuracy in the case study with the different strengths of low signals. Despite its efficacy, there is a significant difference between graph-sc and our scSimGCL, which was evident in the data of de.fracScale 0.1 and 0.15. After zooming on the subgraphs with different dimension sizes, no difference in CA, NMI, and ARI scores of K-Means was observed. This rather intriguing result might be explained by the fact that K-Means lose its power as the number of dimensions increases. Together, these results provide important insights into the flexibility of deep learning-based models, i.e., clustering performance is superior to statistical models under extreme learning settings.

Figure 4 displays the results obtained from the visualization analysis of all baselines and our scSimGCL on the Baron and Zeisel datasets. The difference between scSimGCL and baselines was significant. The identified clusters by our proposed scSimGCL were relatively visible compared to baselines. However, caution must be applied with these identified clusters, as the findings might not be extrapolated to all datasets and learning settings. For example, the identified clusters by deep learning-based models are also known as intermediate representations and are therefore largely affected by model parameters or datasets. This has been illustrated by the results of scGNN on the two datasets.

Figure 5 displays the results of different clustering algorithms on six real scRNA-seq datasets. These results are average values obtained by running all approaches ten times. Our scSimGCL is implemented with K-Means. K-Means, BIRCH, and Agglomerative Clustering can make decisions by indicating "I know" the number of clusters. In contrast, Affinity propagation can make decisions by indicating "I do not know" the number of clusters. The results of K-Means in the first three datasets, such as Shekhar mouse retina cells, are optimal, and those of K-Means in the last three datasets, such as Zeisel, are competitive. There was an observed difference between the performance of K-Means, BIRCH, Agglomerative Clustering, and Affinity propagation. This has been largely illustrated by the weak performance of Affinity propagation on the Shekhar mouse retina cells dataset. The most interesting aspect of this graph is the competitive performance of Agglomerative Clustering on the Camp dataset. It may be that these results benefitted from the size of the input data.

We evaluate our scSimGCL against competing scRNA-seq data imputation approaches on six real scRNA-seq datasets. The scRNA-seq data imputation approaches employed in this study are GE-Impute [37], scGNN [33], AutoClass [14], MAGIC [29], SAVER [10], and scImpute [15]. The GE-Impute is built upon graph neural networks and focuses particularly on scRNA-seq data imputation. Notably, GE-Impute incorporates the cell-cell similarity calculation into the imputation process, which is a crucial factor for improving imputation performance. The AutoClass comprises two neural networks, including an autoencoder and a classifier, which focuses on the provision of scRNA-seq data imputation and cell clustering. The MAGIC is a Markov affinity-based graph imputation of cells that includes a low-rank assumption for data propagation. Accordingly, MAGIC can retain data points in the low-frequency space and filter out noise/dropout points in the high-frequency space. The SAVER is a negative binomial model that imputes dropout values by estimating the distribution of input scRNA-seq data. The scImpute is a statistical model that focuses particularly on scRNA-seq data imputation. The core idea of scImpute is similar to GE-Impute, which imputes dropout values in the gene expression matrix by computing cell-cell similarity. We run all methods ten times and present the average PCCs score.

Figure 6 compares the PCCs score for each approach. We observe that the proposed scSimGCL consistently surpasses the baselines in terms of the PCCs score. Looking at Figure 6, it is apparent that MAGIC is the best baseline that reported significantly more PCCs than the other approaches (except for the result of a dropout rate of 30% in the Camp dataset). Besides, we observed that the imputation accuracy of scGNN and AutoClass in the Baron and Zeisel datasets needs further improvement. The weak performance of deep learning-based models GE-Impute and AutoClass is interesting but not surprising. This result may have something to do with the dropout rate of the input data or the sensitivity and specificity of deep learning-based models.

## Ablation study

We propose three variants of scSimGCL to determine the efficacy of the designed GCL framework. These three variants are termd as scSimGCL$_\alpha$, scSimGCL$_\beta$, and scSimGCL$_\gamma$. In particular, the positive samples for the anchor used in scSimGCL$_\alpha$ are the nodes connected to the anchor and the nodes connected to the anchor from its counterpart view; the positive samples for the anchor used in scSimGCL$_\beta$ are the nodes connected to the anchor and the anchor counterpart in its counterpart view; the positive samples for the anchor used in scSimGCL$_\gamma$ are the anchor counterpart in its counterpart view. We run all methods ten times and present the average CA, NMI, ARI, and PCCs scores. The results of the ablation study are summarized in Figure 7. On average, scSimGCL was shown to have achieved the most satisfactory performance on cell clustering and scRNA-seq data imputation. These results provide further support for the homophily assumption in the graph, which can facilitate the formation of informative positive and negative sample pairs, thereby improving the performance of graph contrastive learning.

We propose a variant of scSimGCL to determine the robustness of decisions in the self-supervised learning setting. The proposed scSimGCL$_\delta$ includes two implementation settings, where $\mathcal{L}^{(gcl)}$ and $\mathcal{L}^{(imp)}$ are separately utilized as the sole objective function in cluster assignment and data imputation. Note that the percentages used in PCCs (10%), PCCs (20%), and PCCs (30%) are dropout rates. We run all methods ten times and present the average CA, NMI, ARI, and PCCs scores. Figure 7 compares CA, NMI, and ARI, PCCs scores for scSimGCL and scSimGCL$_\delta$. Compared with the data in scSimGCL, the performance of scSimGCL$_\delta$ on both cluster assignment and data imputation has a clear decreasing trend. Accordingly, contrastive learning and data imputation in the designed pretraining mechanism are inseparable, which

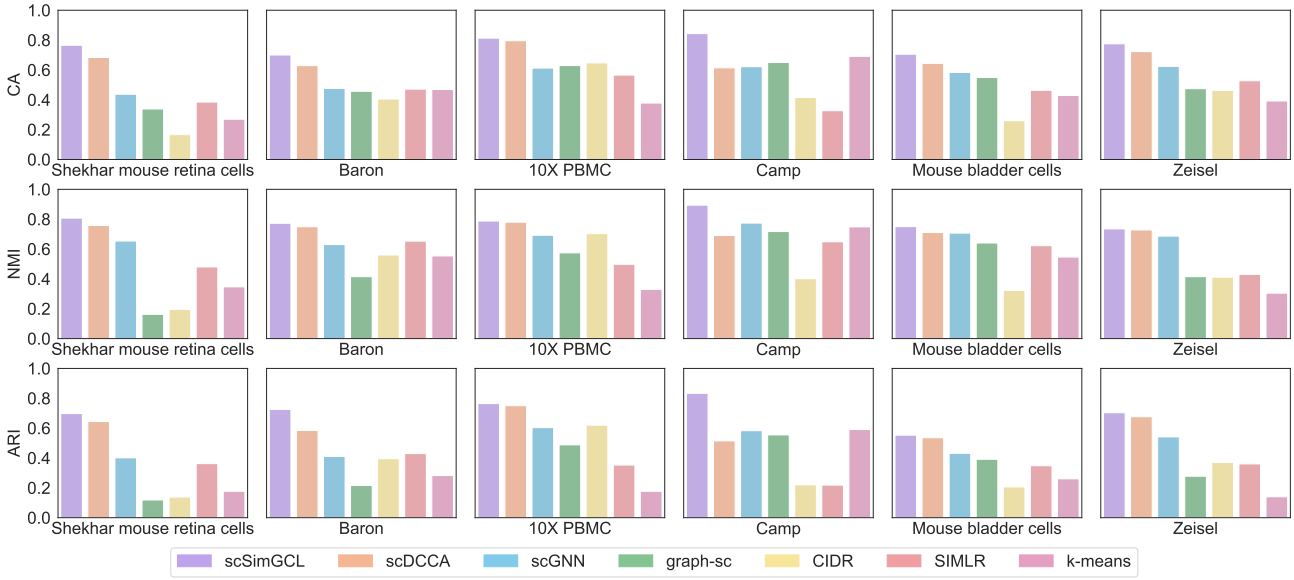


**Fig. 2. Clustering performance comparison in terms of CA, NMI, and ARI on six real scRNA-seq datasets. Higher values indicate better performance.**

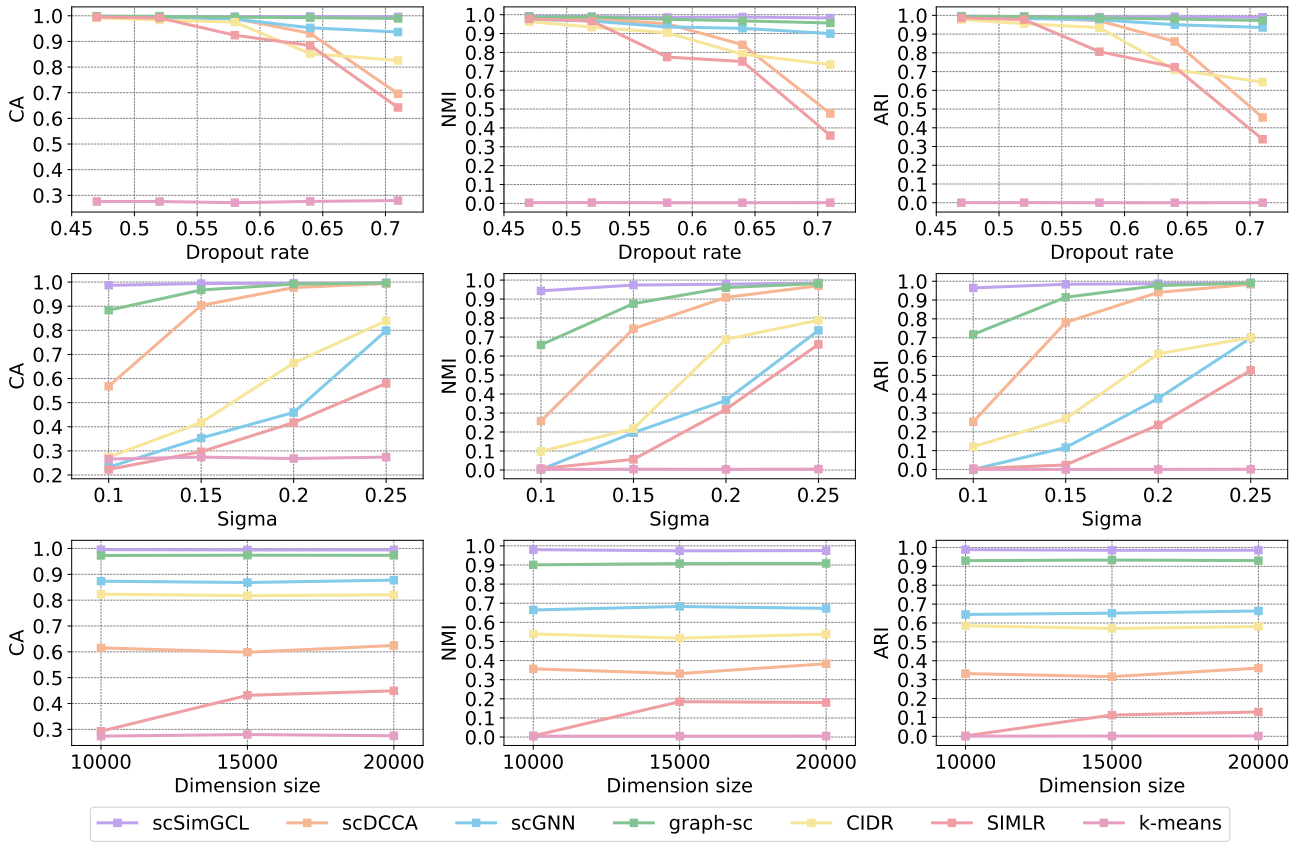


**Fig. 3. Clustering performance comparison in terms of CA, NMI, and ARI on twelve simulated scRNA-seq datasets. Higher values indicate better performance.**

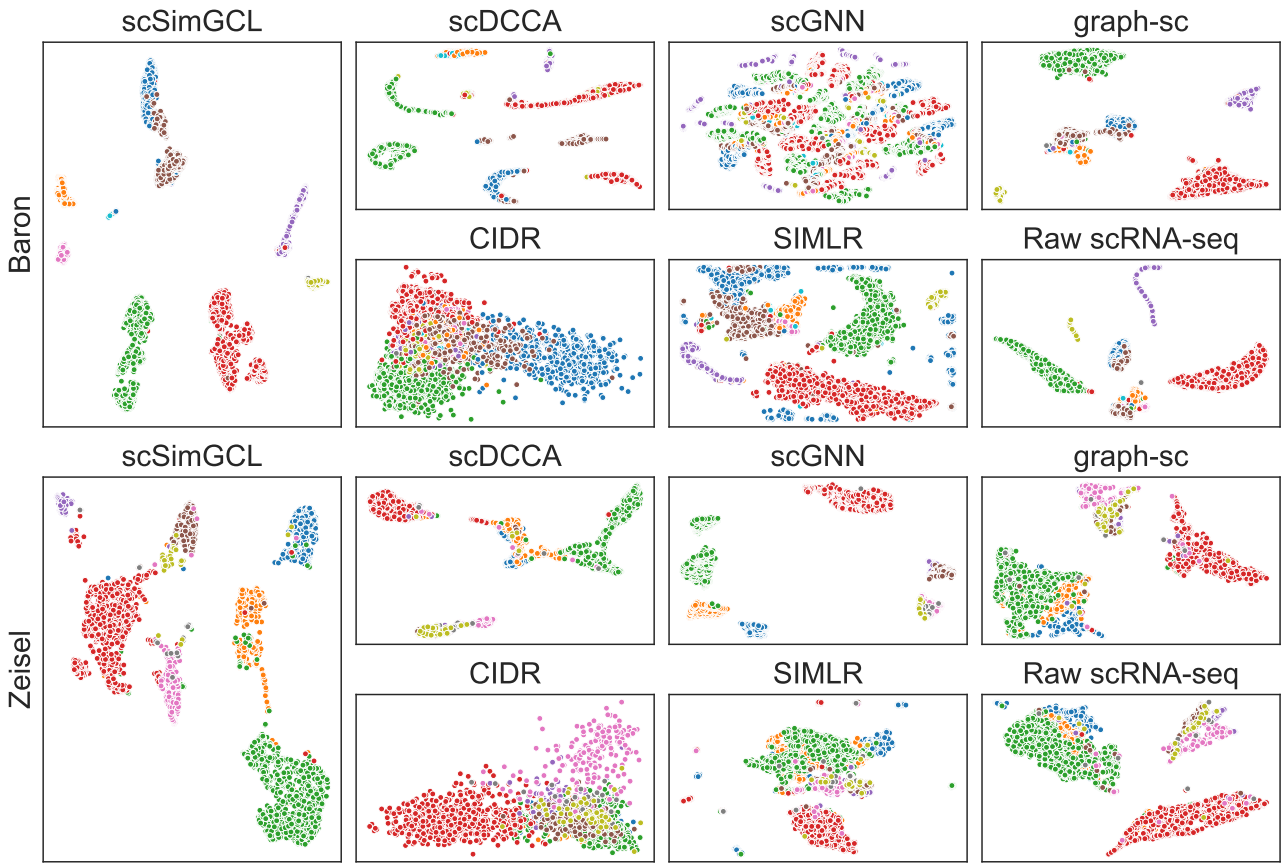


**Fig. 4. Visualization analysis results of baselines and scSimGCL on the Baron and Zeisel datasets.**

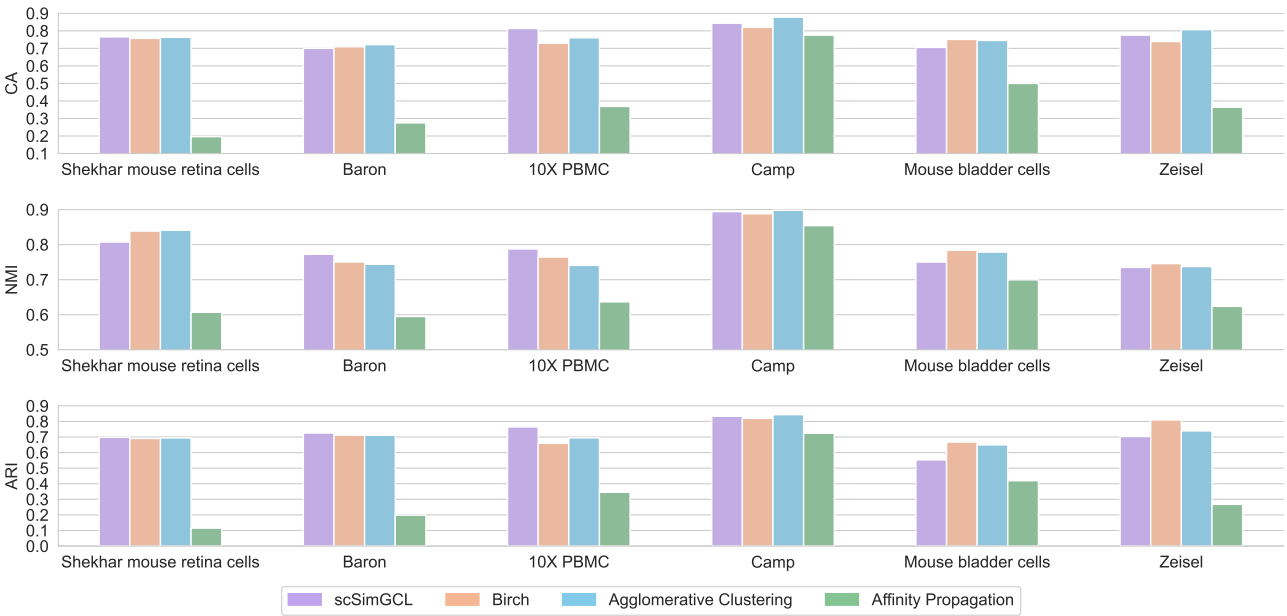


**Fig. 5. Performance comparison results of different clustering algorithms on six real scRNA-seq datasets in terms of CA, NMI, and AR. Higher values indicate better performance.**

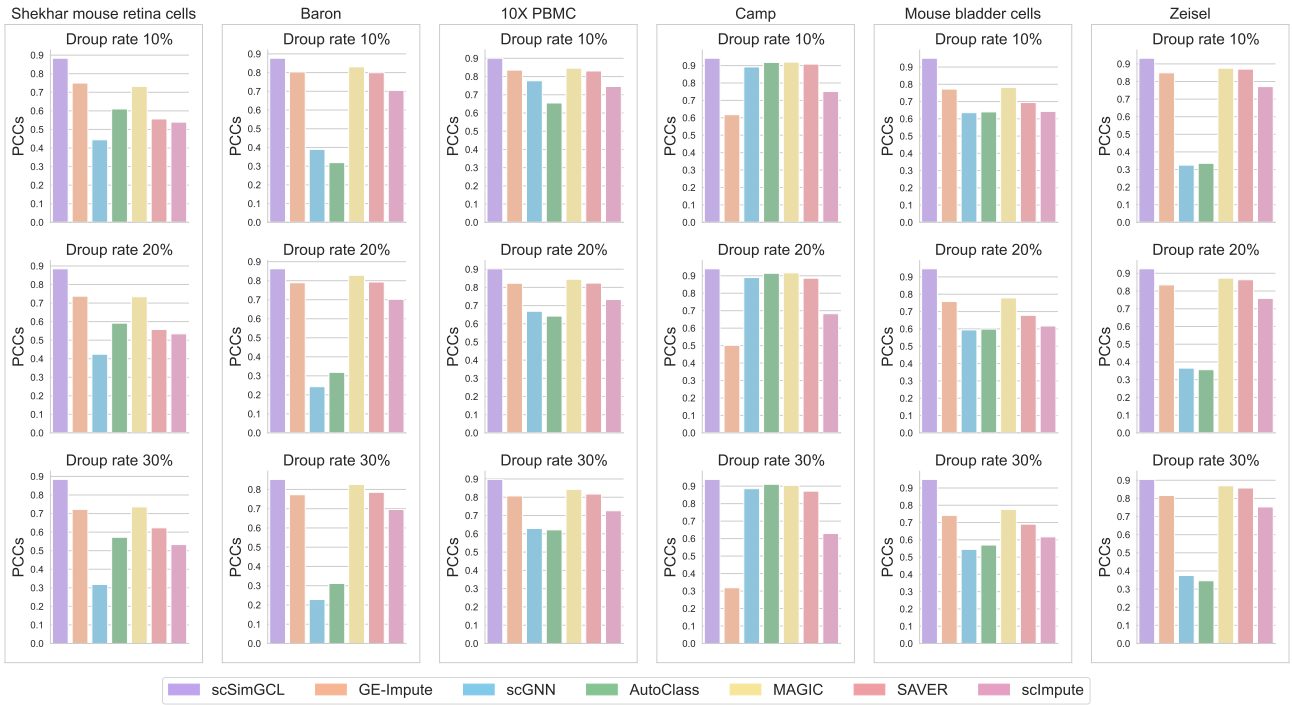


**Fig. 6. Imputation performance comparison results on six real scRNA-seq datasets in terms of PCCs. Higher values indicate better performance.**

is helpful for improving the overall performance of our network architecture.

## Analysis of Hyperparameters

We present a hyperparameter analysis to determine the efficacy of our network architecture. There are batch size, temperature $\tau$, $\phi$, and dropout rate $p^{(drop)}$ that we are interested in. A note of caution is due here since the dropout rate in neural networks differs from that in scRNA-seq datasets. Batch size and dropout rate have long been a question of great interest in neural networks. Temperature parameter is often used in research on contrastive learning. Note that varied batch sizes are implemented using three datasets with a relatively large sample size, as shown in Figure 8. These results are average values obtained by running scSimGCL with different parameters ten times. After zooming on the subgraphs with varied batch sizes, we observed that PCCs in the three datasets can reach the optimal value on the same batch size. In the same vein, CA, NMI, and ARI in the Shekhar mouse retina cells and 10X PBMC datasets can reach optimal values on the same batch size. As can be seen from the subgraphs (below), our approach could make decisions based on varied parameters $\phi$, $\tau$, and $p^{(drop)}$. This analysis was successful as it was able to identify patterns and trends in the data.

# Conclusion

Single-cell RNA sequencing has become the most popular method for investigating transcriptome-wide gene expression at the single-cell level. Using scRNA-seq data on cell clustering is a well-established approach to provide a detailed understanding of the groups of cells with similar expression profiles. To achieve this aim, we need to solve challenges stemming from raw scRNA-seq data, including high dimensionality and dropout phenomenon. The existing deep learning-based solutions for addressing these challenges are extensive and focus particularly on graph machine learning models and contrastive learning-based models. There is still much work to be done to achieve desirable representations and accuracy simultaneously.

This study set out to marry graph neural networks with contrastive learning for scRNA-seq data analysis. We propose scSimGCL, a simple and effective framework based on the graph contrastive learning paradigm that leverages self-supervised pretraining of graph neural networks to generate high-quality representations critical for cell clustering. Extensive experiments were carried out on simulated and real scRNA-seq datasets. Our scSimGCL demonstrated significant improvement in scRNA-seq data imputation and cell clustering. The results of clustering assignment analysis indicated that scSimGCL is a general approach that can include competing clustering algorithms. Ablation study and hyperparameter analysis further confirmed the efficacy of our network architecture with the robustness of decisions in the self-supervised learning setting.

With regard to the research method, a major limitation needs to be acknowledged here, i.e., the lack of uncertainty estimation in model decisions (associated with the over-confidence problem in deep learning approaches) adds caution regarding the generalizability of findings. Further modeling work will have to be conducted in order to improve the transparency of scSimGCL, such as developing interpretable and reliable analytical approaches. Further experiments using a broader range of scRNA-seq data could establish the efficiency of scSimGCL.

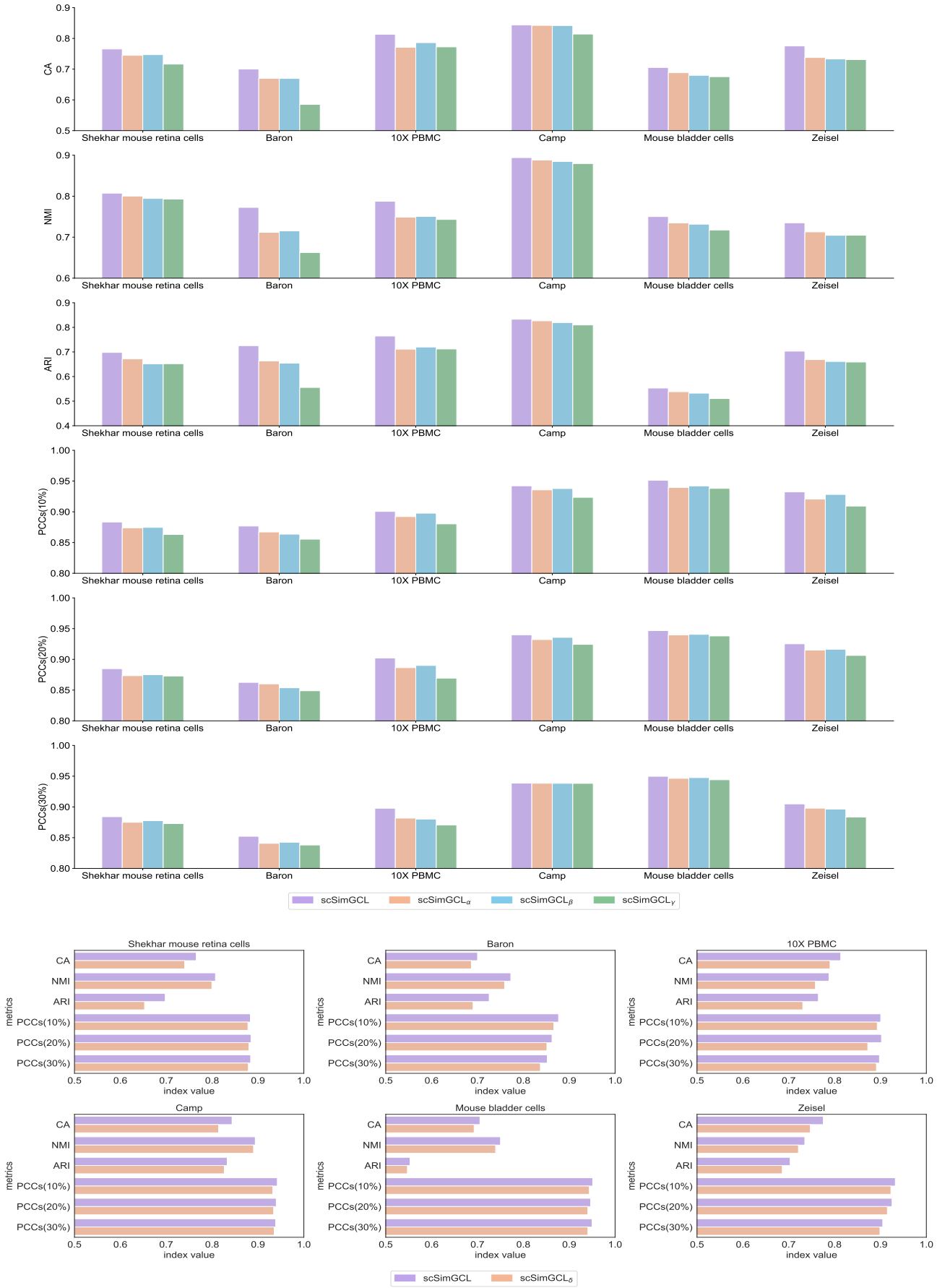


**Fig. 7. Performance comparison results between scSimGCL and its three variants.**

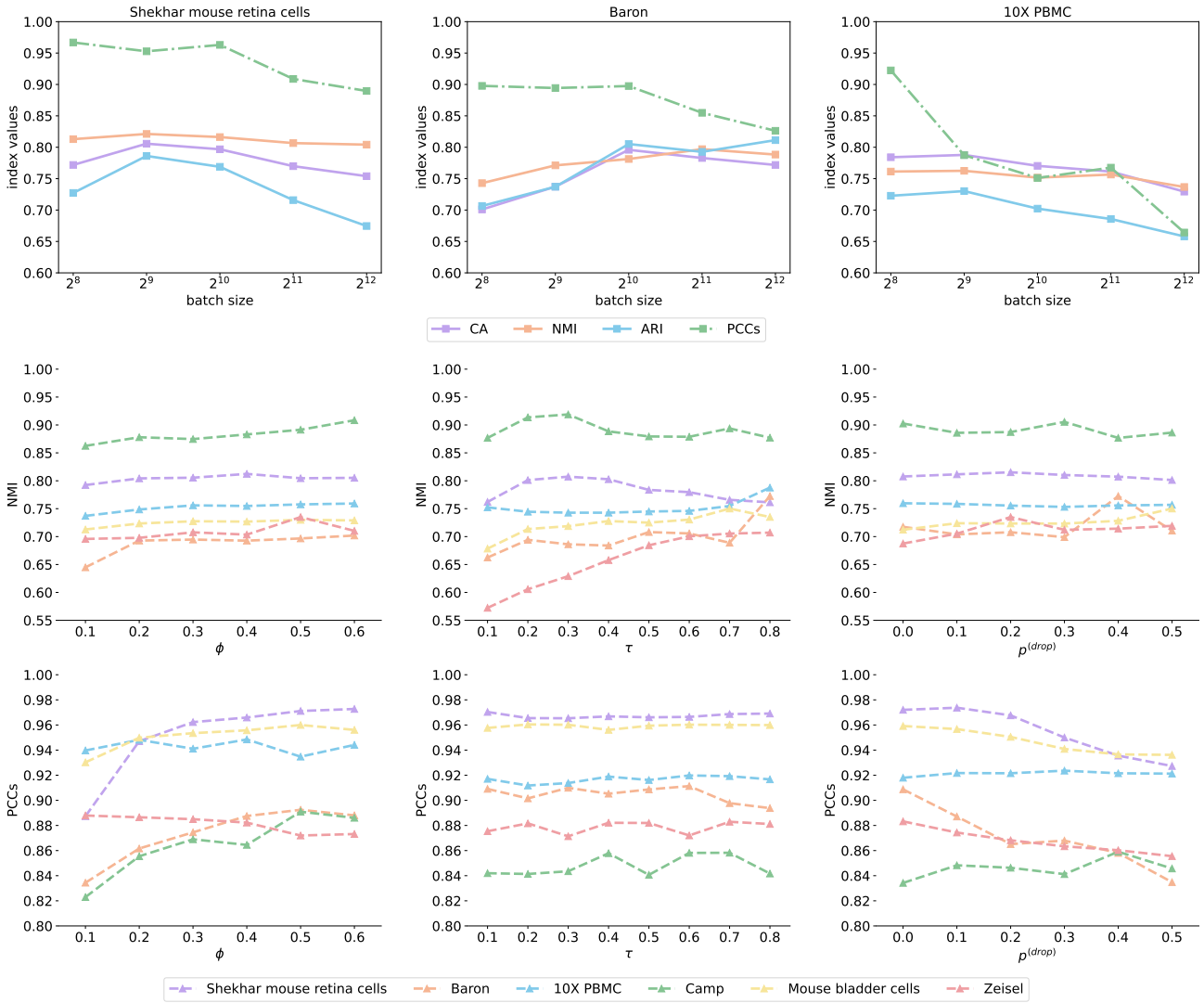


**Fig. 8. Hyperparameter analysis results in terms of CA, NMI, ARI, and PCCs. Higher values indicate better performance.**

**Key Points**

- scSimGCL is a simple and effective graph contrastive learning framework for learning high-quality representations crucial for robust cell clustering.
- scSimGCL outperforms competing state-of-the-art models in scRNA-seq data imputation and cell clustering by a significant margin.
- scSimGCL is capable of making informed decisions by indicating "I know" and "I do not know" the number of clusters, which is a critical aspect in unsupervised learning settings for scRNA-seq data analysis.
- scSimGCL represents a further step towards developing a foundation model for cell clustering.

## Funding

This work is supported by the National Key Research and Development Program of China (No. 2022YFF1000100), the National Natural Science Foundation of China (No. 62202388), the Qin Chuangyuan Innovation and Entrepreneurship Talent Project (No. QCYRCXM-2022-230), and the Talent Research Funding at Northwest A&F University (No. Z1090222021).

## Competing interests

None declared.

## Data availability

The scRNAseq data that support the findings of this paper are publicly available at GitHub: `https://github.com/zhangzh1328/scSimGCL`.

## Code availability

The proposed scSimGCL is developed using Python 3.8.17 with the deep learning framework PyTorch 1.8.1. The source code of scSimGCL is publicly available at `https://github.com/zhangzh1328/scSimGCL`.

## References


1. Aisha A AlJanahi, Mark Danielsen, and Cynthia E Dunbar. An introduction to the analysis of single-cell rna-sequencing data. *Molecular Therapy Methods & Clinical Development*, 10:189–196, 2018.
2. Maayan Baron, Adrian Veres, Samuel L Wolock, Aubrey L Faust, Renaud Gaujoux, Amedeo Vetere, Jennifer Hyoje Ryu, Bridget K Wagner, Shai S Shen-Orr, Allon M Klein, et al. A single-cell transcriptomic map of the human and mouse pancreas reveals inter-and intra-cell population structure. *Cell systems*, 3(4):346–360, 2016.
3. J Gray Camp, Keisuke Sekine, Tobias Gerber, Henry Loeffler-Wirth, Hans Binder, Malgorzata Gac, Sabina Kanton, Jorge Kageyama, Georg Damm, Daniel Seehofer, et al. Multilineage communication regulates human liver bud development from pluripotency. *Nature*, 546(7659):533–538, 2017.
4. Yi Cheng and Xiuli Ma. scgac: a graph attentional architecture for clustering single-cell rna-seq data. *Bioinformatics*, 38(8):2187–2193, 2022.
5. Madalina Ciortan and Matthieu Defrance. Contrastive self-supervised clustering of scrna-seq data. *BMC bioinformatics*, 22(1):280, 2021.
6. Madalina Ciortan and Matthieu Defrance. Gnn-based embedding for clustering scrna-seq data. *Bioinformatics*, 38(4):1037–1044, 2022.
7. Gökcen Eraslan, Lukas M Simon, Maria Mircea, Nikola S Mueller, and Fabian J Theis. Single-cell rna-seq denoising using a deep count autoencoder. *Nature communications*, 10(1):390, 2019.
8. Yanglan Gan, Yuhan Chen, Guangwei Xu, Wenjing Guo, and Guobing Zou. Deep enhanced constraint clustering based on contrastive learning for scrna-seq data. *Briefings in Bioinformatics*, 24(4):bbad222, 2023.
9. Xiaoping Han, Renying Wang, Yincong Zhou, Lijiang Fei, Huiyu Sun, Shujing Lai, Assieh Saadatpour, Ziming Zhou, Haide Chen, Fang Ye, et al. Mapping the mouse cell atlas by microwell-seq. *Cell*, 172(5):1091–1107, 2018.
10. Mo Huang, Jingshu Wang, Eduardo Torre, Hannah Dueck, Sydney Shaffer, Roberto Bonasio, John I Murray, Arjun Raj, Mingyao Li, and Nancy R Zhang. Saver: gene expression recovery for single-cell rna sequencing. *Nature methods*, 15(7):539–542, 2018.
11. Lawrence Hubert and Phipps Arabie. Comparing partitions. *Journal of classification*, 2:193–218, 1985.
12. Thomas N Kipf and Max Welling. Semi-supervised classification with graph convolutional networks. *arXiv preprint arXiv:1609.02907*, 2016.
13. Junseok Lee, Sungwon Kim, Dongmin Hyun, Namkyeong Lee, Yejin Kim, and Chanyoung Park. Deep single-cell rna-seq data clustering with graph prototypical contrastive learning. *Bioinformatics*, 39(6):btad342, 2023.
14. Hui Li, Cory R Brouwer, and Weijun Luo. A universal deep neural network for in-depth cleaning of single-cell rna-seq data. *Nature Communications*, 13(1):1901, 2022.
15. Wei Vivian Li and Jingyi Jessica Li. An accurate and robust imputation method scimpute for single-cell rna-seq data. *Nature communications*, 9(1):997, 2018.
16. Xiangjie Li, Kui Wang, Yafei Lyu, Huize Pan, Jingxiao Zhang, Dwight Stambolian, Katalin Susztak, Muredach P Reilly, Gang Hu, and Mingyao Li. Deep learning enables accurate clustering with batch effect removal in single-cell rna-seq analysis. *Nature communications*, 11(1):2338, 2020.
17. Peijie Lin, Michael Troup, and Joshua WK Ho. Cidr: Ultrafast and accurate clustering through imputation for single-cell rna-seq data. *Genome biology*, 18:1–11, 2017.
18. Yixin Liu, Yu Zheng, Daokun Zhang, Hongxu Chen, Hao Peng, and Shirui Pan. Towards unsupervised deep graph structure learning. In *Proceedings of the ACM Web Conference 2022*, pages 1392–1403, 2022.
19. Michael Moor, Oishi Banerjee, Zahra Shakeri Hossein Abad, Harlan M Krumholz, Jure Leskovec, Eric J Topol, and Pranav Rajpurkar. Foundation models for generalist medical artificial intelligence. *Nature*, 616(7956):259–265, 2023.
20. Cheng Peng, Xi Yang, Mengxian Lyu, Kaleb E Smith, Mona G Flores, Jiang Bian, and Yonghui Wu. Gatortron and gatortrongpt: Large language models for clinical narratives. In *AAAI 2024 Spring Symposium on Clinical Foundation Models*, 2024.
21. Peng Qiu. Embracing the dropouts in single-cell rna-seq analysis. *Nature communications*, 11(1):1169, 2020.
22. Karthik Shekhar, Sylvain W Lapan, Irene E Whitney, Nicholas M Tran, Evan Z Macosko, Monika Kowalczyk, Xian Adiconis, Joshua Z Levin, James Nemesh, Melissa Goldman, et al. Comprehensive classification of retinal bipolar neurons by single-cell transcriptomics. *Cell*, 166(5):1308–1323, 2016.
23. Alexander Strehl and Joydeep Ghosh. Cluster ensembles—a knowledge reuse framework for combining multiple partitions. *Journal of machine learning research*, 3(Dec):583–617, 2002.
24. Sheng-Wen Tian, Jian-Cheng Ni, Yu-Tian Wang, Chun-Hou Zheng, and Cun-Mei Ji. scgcc: Graph contrastive clustering with neighborhood augmentations for scrna-seq data analysis. *IEEE Journal of Biomedical and Health Informatics*, 2023.
25. Tian Tian, Ji Wan, Qi Song, and Zhi Wei. Clustering single-cell rna-seq data with a model-based deep learning approach. *Nature Machine Intelligence*, 1(4):191–198, 2019.
26. Tian Tian, Jie Zhang, Xiang Lin, Zhi Wei, and Hakon Hakonarson. Model-based deep embedding for constrained clustering analysis of single cell rna-seq data. *Nature communications*, 12(1):1873, 2021.
27. Yonglong Tian, Chen Sun, Ben Poole, Dilip Krishnan, Cordelia Schmid, and Phillip Isola. What makes for good views for contrastive learning? *Advances in neural information processing systems*, 33:6827–6839, 2020.
28. Bram Van de Sande, Joon Sang Lee, Euphemia Mutasa-Gottgens, Bart Naughton, Wendi Bacon, Jonathan Manning, Yong Wang, Jack Pollard, Melissa Mendez, Jon Hill, et al. Applications of single-cell rna sequencing in drug discovery and development. *Nature Reviews Drug Discovery*, 22(6):496–520, 2023.
29. David Van Dijk, Roshan Sharma, Juozas Nainys, Kristina Yim, Pooja Kathail, Ambrose J Carr, Cassandra Burdziak, Kevin R Moon, Christine L Chaffer, Diwakar Pattabiraman,

et al. Recovering gene interactions from single-cell data using data diffusion. *Cell*, 174(3):716–729, 2018.

30. Ashish Vaswani, Noam Shazeer, Niki Parmar, Jakob Uszkoreit, Llion Jones, Aidan N Gomez, Łukasz Kaiser, and Illia Polosukhin. Attention is all you need. *Advances in neural information processing systems*, 30, 2017.
31. Bo Wang, Junjie Zhu, Emma Pierson, Daniele Ramazzotti, and Serafim Batzoglou. Visualization and analysis of single-cell rna-seq data by kernel-based similarity learning. *Nature methods*, 14(4):414–416, 2017.
32. Jing Wang, Junfeng Xia, Haiyun Wang, Yansen Su, and Chun-Hou Zheng. scdcca: deep contrastive clustering for single-cell rna-seq data based on auto-encoder network. *Briefings in Bioinformatics*, 24(1):bbac625, 2023.
33. Juexin Wang, Anjun Ma, Yuzhou Chang, Jianting Gong, Yuexu Jiang, Ren Qi, Cankun Wang, Hongjun Fu, Qin Ma, and Dong Xu. scgnn is a novel graph neural network framework for single-cell rna-seq analyses. *Nature communications*, 12(1):1882, 2021.
34. Shudong Wang, Yu Zhang, Yulin Zhang, Wenhao Wu, Lan Ye, YunYin Li, Jionglong Su, and Shanchen Pang. scasgc: An adaptive simplified graph convolution model for clustering single-cell rna-seq data. *Computers in Biology and Medicine*, 163:107152, 2023.
35. F Alexander Wolf, Philipp Angerer, and Fabian J Theis. Scanpy: large-scale single-cell gene expression data analysis. *Genome biology*, 19:1–5, 2018.
36. Michael Wornow, Yizhe Xu, Rahul Thapa, Birju Patel, Ethan Steinberg, Scott Fleming, Michael A Pfeffer, Jason Fries, and Nigam H Shah. The shaky foundations of large language models and foundation models for electronic health records. *npj Digital Medicine*, 6(1):135, 2023.
37. Xiaobin Wu and Yuan Zhou. Ge-impute: graph embedding-based imputation for single-cell rna-seq data. *Briefings in Bioinformatics*, 23(5):bbac313, 2022.
38. Junyuan Xie, Ross Girshick, and Ali Farhadi. Unsupervised deep embedding for clustering analysis. In *International conference on machine learning*, pages 478–487. PMLR, 2016.
39. Zehao Xiong, Jiawei Luo, Wanwan Shi, Ying Liu, Zhongyuan Xu, and Bo Wang. scgcl: an imputation method for scrna-seq data based on graph contrastive learning. *Bioinformatics*, 39(3):btad098, 2023.
40. Fan Yang, Wenchuan Wang, Fang Wang, Yuan Fang, Duyu Tang, Junzhou Huang, Hui Lu, and Jianhua Yao. scbert as a large-scale pretrained deep language model for cell type annotation of single-cell rna-seq data. *Nature Machine Intelligence*, 4(10):852–866, 2022.
41. Bin Yu, Chen Chen, Ren Qi, Ruiqing Zheng, Patrick J Skillman-Lawrence, Xiaolin Wang, Anjun Ma, and Haiming Gu. scgmai: a gaussian mixture model for clustering single-cell rna-seq data based on deep autoencoder. *Briefings in bioinformatics*, 22(4):bbaa316, 2021.
42. Luke Zappia, Belinda Phipson, and Alicia Oshlack. Splatter: simulation of single-cell rna sequencing data. *Genome biology*, 18(1):174, 2017.
43. Amit Zeisel, Ana B Muñoz-Manchado, Simone Codeluppi, Peter Lönnerberg, Gioele La Manno, Anna Juréus, Sueli Marques, Hermany Munguba, Liqun He, Christer Betsholtz, et al. Cell types in the mouse cortex and hippocampus revealed by single-cell rna-seq. *Science*, 347(6226):1138–1142, 2015.
44. Tong Zhao, Wei Jin, Yozen Liu, Yingheng Wang, Gang Liu, Stephan Günnemann, Neil Shah, and Meng Jiang. Graph data augmentation for graph machine learning: A survey. *arXiv preprint arXiv:2202.08871*, 2022.
45. Grace XY Zheng, Jessica M Terry, Phillip Belgrader, Paul Ryvkin, Zachary W Bent, Ryan Wilson, Solongo B Ziraldo, Tobias D Wheeler, Geoff P McDermott, Junjie Zhu, et al. Massively parallel digital transcriptional profiling of single cells. *Nature communications*, 8(1):14049, 2017.
46. Zilu Zhou, Bihui Xu, Andy Minn, and Nancy R Zhang. Dendro: genetic heterogeneity profiling and subclone detection by single-cell rna sequencing. *Genome biology*, 21:1–15, 2020.